Volume 126, Article No. 126032 (2021) https://doi.org/10.6028/jres.126.032
Journal of Research of National Institute of Standards and Technology

Ratio-Based Pulse Shape Discrimination: Analytic Results for Gaussian and Poisson Noise Models

Kevin J Coakley

National Institute of Standards and Technology,
Boulder, CO 80305, USA

kevin.coakley@nist.gov

In experiments in a range of fields including fast neutron spectroscopy and astroparticle physics, one can discriminate events of interest from background events based on the shapes of electronic pulses produced by energy deposits in a detector. Here, I focus on a well-known pulse shape discrimination method based on the ratio of the temporal integral of the pulse over an early interval X_p and the temporal integral over the entire pulse X_t. For both event classes, for both a Gaussian noise model and a Poisson noise model, I present analytic expressions for the conditional distribution of X_p given knowledge of the observed value of X_t and a scaled energy deposit corresponding to the product of the full energy deposit and a relative yield factor. I assume that the energy-dependent theoretical prompt fraction for both classes are known exactly. With a Bayesian approach that accounts for imperfect knowledge of the scaled energy deposit, I determine the posterior mean background acceptance probability given the target signal acceptance probability as a function of the observed value of X_t. My method enables one to determine receiver-operating-characteristic curves by numerical integration rather than by Monte Carlo simulation for these two noise models.

Key words: Bayesian analysis; classification; Gaussian processes; Poisson processes, prompt fraction statistic; pulse shape discrimination; receiver-operating-characteristic curve.

Accepted: August 16, 2021

Published: November 9, 2021

https://doi.org/10.6028/jres.126.032

1. Introduction

In a variety of experiments in fields such as astroparticle physics (for example, see Refs. [1–6]), fast neutron spectroscopy [7–10], and neutrino physics (for example, see Refs. [11–13]), events of interest and background events deposit energy in detectors. Typically, the shapes of measured electronic pulses generated by events of interest and background events are different. There are many different methods [14] for pulse shape discrimination (PSD), including those based on: ratios of pulse integrals corresponding to different time intervals [8, 15], comparison to reference templates [16–18], machine learning [19–25], pulse gradient methods [26], zero-crossing analysis [27, 28], frequency gradient analysis [29], and Fourier transform analysis [30]. Here, I focus on a "prompt fraction" discrimination statistic F_p defined as

$$F_p = \frac{X_p}{X_t}, \tag{1}$$

where X_p is the integrated pulse in a prompt time interval $[T_{begin}, T_{prompt}]$, and X_t is the integrated pulse in a total time interval $[T_{begin}, T_{end}]$. I consider two cases. In one case, X_p and X_t are correlated Gaussian random variables. In the other case, X_p and X_t are correlated Poisson random variables.

How to cite this article:
Coakley KJ (2021) Ratio-Based Pulse Shape Discrimination: Analytic Results for Gaussian and Poisson Noise Models. *J Res Natl Inst Stan* 126:126032. https://doi.org/10.6028/jres.126.032.

There are exact and nearly exact approximations for the distribution of the ratio of Gaussian (normal) random variables with known means, variances, and correlation [31–33]. Based on Refs. [31, 32], the work in Ref. [34] includes a model to predict the distribution of prompt fraction statistics produced by a given energy deposit where the observed values of X_p and X_t are unconstrained. In applications of interest, data generated by a continuum of energy deposits are binned according to observed values of X_t. Thus, the conditional distribution of X_p given the measured value of X_t is of primary interest for PSD studies and the focus of this work.

In many experimental studies, only a fraction of the energy deposited in a detector produces a measurement of interest. In general, this fraction varies for the two event classes. In this work, for each class, I assume that this fraction does not vary from event-to-event. Based on these fractions, I assign a relative yield factor β to each class. For the class with the higher fraction, $\beta = 1$. For the other class, $0 < \beta \leq 1$. If both classes have the same fraction, $\beta = 1$ for both classes. Given the full energy deposit e_{dep} and β, I define a scaled energy deposit e as:

$$e = \beta e_{dep}. \tag{2}$$

For any scaled energy deposit e, I assume that the expected value of X_t is the same for both event classes.

For Gaussian and Poisson noise models, I derive exact expressions for the conditional distributions of X_p given the measured value of X_t and the unobserved value of e. The major technical step to get the analytical result for the Poisson case is well known, but the major technical step to get the analytical result for the Gaussian case is, to the best of my knowledge, a new contribution to the PSD literature. In general, the source that generates events for each class has a potentially broad energy deposit spectrum. For the Poisson case, for each event class, I assume knowledge of the Poisson parameters for a prompt time interval and a late time interval as a function of e. For the Gaussian case, for each event class, I assume knowledge of the mean and variance of the integrated pulse for both a prompt time interval and a late time interval as a function of e. For the cases studied, I assign an event to the signal class if the observed value of X_p exceeds a selected discrimination threshold that in general depends on the observed value of X_t. With a Bayesian method, I determine the posterior mean background acceptance probability as well as the posterior mean signal acceptance probability. My methods should facilitate evaluation of receiver-operating-characteristic curves (signal acceptance probability versus background acceptance probability) [35] for the Gaussian and Poisson cases.

2. Gaussian Noise Model

2.1 Conditional Distribution of X_p

Throughout this work, I denote a random variable with a capital letter (e.g. X) and a particular realization of the random variable with a lower case letter (e.g. x). The prompt fraction statistic is a random variable $F_p = \frac{X_p}{X_t}$. I decompose X_t into the sum of a prompt and late contribution, i.e.,

$$X_t = X_p + X_l, \tag{3}$$

where X_p is the integrated pulse measured during $[T_{begin}, T_{prompt}]$, and X_l is the integrated pulse measured during $(T_{prompt}, T_{end}]$. Here, I assume that X_p and X_l are independent Gaussian random variables with known energy-dependent means $\mu_p(e)$ and $\mu_l(e)$, and known energy-dependent variances $\sigma_p^2(e)$ and $\sigma_l^2(e)$. Given these assumptions, the expected value and variance of X_t are

$$\mu_t(e) = \mu_p(e) + \mu_l(e), \tag{4}$$

and

$$\sigma_t^2(e) = \sigma_p^2(e) + \sigma_l^2(e). \tag{5}$$

Further, the correlation ρ between X_p and X_t is

$$\rho(e) = \frac{\mathbb{E}(\ \ (X_p - \mu_p(e))\ (X_t - \mu_t(e))\ \ )}{\sigma_p(e)\sigma_t(e)} = \frac{\sigma_p(e)}{\sigma_t(e)}. \tag{6}$$

As discussed in many references including Ref. [36], if two Gaussian random variables X and Y have correlation ρ, the distribution of the conditional value of Y given the observed value of X, $(Y|X = x)$, is a Gaussian random variable with expected value

$$\mathbb{E}(Y|X = x) = \mathbb{E}(Y) + \rho\frac{\sigma_Y}{\sigma_X}(x - \mathbb{E}(X)), \tag{7}$$

and variance

$$\mathrm{Var}(Y|X = x) = (1 - \rho^2)\mathrm{Var}(Y). \tag{8}$$

Hence, for the mono-energetic case, given that the observed value of X_t is x_t and the scaled energy deposit is e, X_p is a Gaussian random variable with expected value

$$\mathbb{E}(X_p|X_t = x_t, E = e) = \mu_p(x_t, e) = \mu_p(e) + \frac{\sigma_p^2(e)}{\sigma_t^2(e)}(x_t - \mu_t(e)), \tag{9}$$

and variance

$$\mathrm{Var}(X_p|X_t = t, E = e) = \sigma_p^2(x_t, e) = \sigma_p^2(e)(\ 1 - \frac{\sigma_p^2(e)}{\sigma_t^2(e)}\ ). \tag{10}$$

2.2 Acceptance Probabilities

Without loss of generality, I assume that events produced by the signal of interest yield, on average, larger observations of X_p (compared to background events) for any particular scaled energy deposit e. Given this assumption, a natural classification rule is to assign an event to the signal class if the observed value of X_p exceeds a discrimination threshold $c(x_t)$ that depends on the observed value of X_t. In general, many scientific considerations influence the choice of the discrimination threshold $c(x_t)$. Given that $F(\ x, \mu, \sigma\ )$ is the cumulative distribution function (at x) for a Gaussian random variable with mean μ and standard deviation σ, the background acceptance probability, $p_{BG}(x_t, e)$, is

$$p_{BG}(x_t, e) = 1 - F(\ c(x_t),\ \mu_p(x_t, e, B),\ \sigma_p(x_t, e, B)\ ), \tag{11}$$

where $\mu_p(x_t, e, B)$ is the Eq. (9) prediction of $\mu_p(x, e)$ for the background class, and $\sigma_p(x_t, e, B)$ is the Eq. (10) prediction of $\sigma_p(x_t, e)$ for the background class. The signal acceptance probability is

$$p_S(x_t, e) = 1 - F(\ c(x_t),\ \mu_p(x_t, e, S),\ \sigma_p(x_t, e, S)\ ), \tag{12}$$

where $\mu_p(x_t, e, S)$ and $\sigma_p(x_t, e, S)$ correspond to the Eq. (9) and Eq. (10) predictions for the signal class.

2.2.1 Posterior Means of Acceptance Probabilities

I account for uncertainty in the scaled energy deposit that produces any particular event with a Bayesian method. For a comprehensive review of Bayesian methods, see Ref. [37]. For the ideal case where one has an exact model for the scaled energy deposit spectrum due to background events, the prior distribution for the scaled energy deposit would be equated to this spectrum. However, in general, such an exact model may not be available. For the general case, the prior distribution would be selected by scientific judgement.

I denote the prior distribution for the scaled energy deposit due to a background event as $\pi_{BG}(e)$. For the Gaussian noise model, the conditional probability density function of X_t given that $E = e$ is

$$f_d(X_t = x_t|e) = \frac{1}{\sqrt{2\pi}\sigma_T(e)} \exp(-\frac{(x_t - \mu_T(e))^2}{2\sigma_T^2(e)}). \tag{13}$$

Without loss of generality, I assume that $\mu_T(e)$ and $\sigma_T(e)$ are the same for both the signal class and the background class. By Bayes' theorem, the posterior distribution for E given $X_t = x_t$ for a background event is

$$f_e(e|x_t) = \frac{f_d(x_t|e)\pi_{BG}(e)}{\int_e f_d(x_t|e)\pi_{BG}(e)de}. \tag{14}$$

Hence, given x_t, the posterior mean of the acceptance probability for the background class is

$$\bar{p}_{BG}(x_t) = \int_e p_{BG}(x_t,e) f_e(e|x_t)de. \tag{15}$$

By similar methods, one can derive the posterior mean of the acceptance probability for the signal class as

$$\bar{p}_S(x_t) = \int_e p_S(x_t,e) f_e(e|x_t)de. \tag{16}$$

As a caveat, if the prior distribution for the scaled energy deposit for the signal class differs from $\pi_{BG}(e)$, $f_e(e|x_t)$ in Eq. (16) would differ from the corresponding expression in Eq. (15).

2.3 Simulation Study

I assume that energies and integrated voltage pulses are dimensionless. As an illustrative example, I assume that $\beta = 1$ [see Eq. (2)] for both classes, and that

$$\mu_p(e) = e\ (\ \alpha + \beta(\ \ 1 - \exp(-\frac{e}{200})\ \ )\ ), \tag{17}$$

$$\mu_t(e) = e, \tag{18}$$

and

$$\mu_l(e) = e - \mu_p(e). \tag{19}$$

For the signal class, (α,β) = (0.6,0.1). For the background class, (α,β) = (0.5,-0.1) (see Fig. 1). For both classes,

$$\sigma_l^2(e)\ =\ 2\mu_l(e)\ +\ 1, \tag{20}$$

and

$$\sigma_p^2(e)\ =\ 2\mu_p(e)\ +\ 1. \tag{21}$$

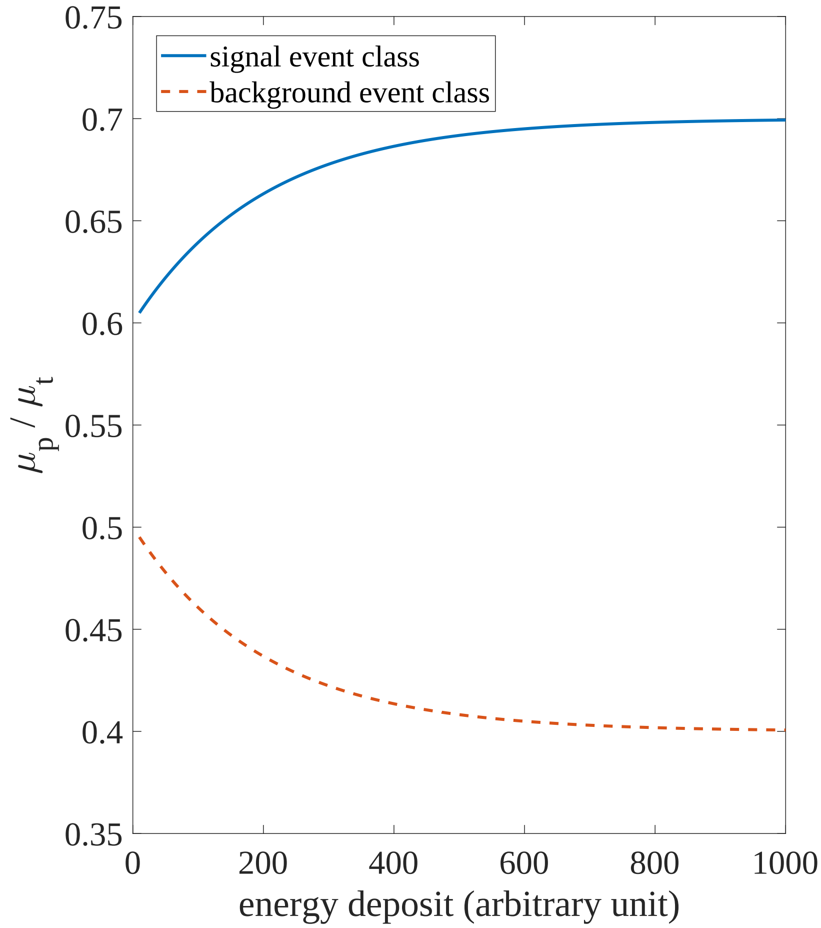

Fig. 1. The theoretical prompt fraction, μ_p/μ_t, varies with the energy deposit for both classes in the simulation experiment. Because the relative yield term β equals 1 for both classes, the scaled energy deposit [see Eq. (2)] and energy deposit agree in this study.

Given the observed value x_t, I estimate e to be $\hat{e} = x_t$. In the primary studies presented here, I set the discrimination threshold $c(x_t)$ to be the expected value of $(X_p|X_t = x_t, E = \hat{e})$ for signal events [see Eq. (9)]. This choice corresponds to a target signal acceptance of 0.5. Since $\mu_t(e = x_t) = x_t$, $c(x_t) = \mu_p(e = x_t)$.

In Fig. 2, I illustrate my method for the case where $x_t = 200$ and the prior distribution for e, $\pi_{BG}(e)$, is uniform for the range $10 \le e \le 1000$. At other values of e, the prior distribution is 0. I also determine results for a truncated exponential prior distribution for the range $10 \le e \le 1000$ where

$$\pi_{BG}(e) \propto \exp(-\frac{e}{500}). \tag{22}$$

At other values of e, the prior distribution is 0 (see Table 1).

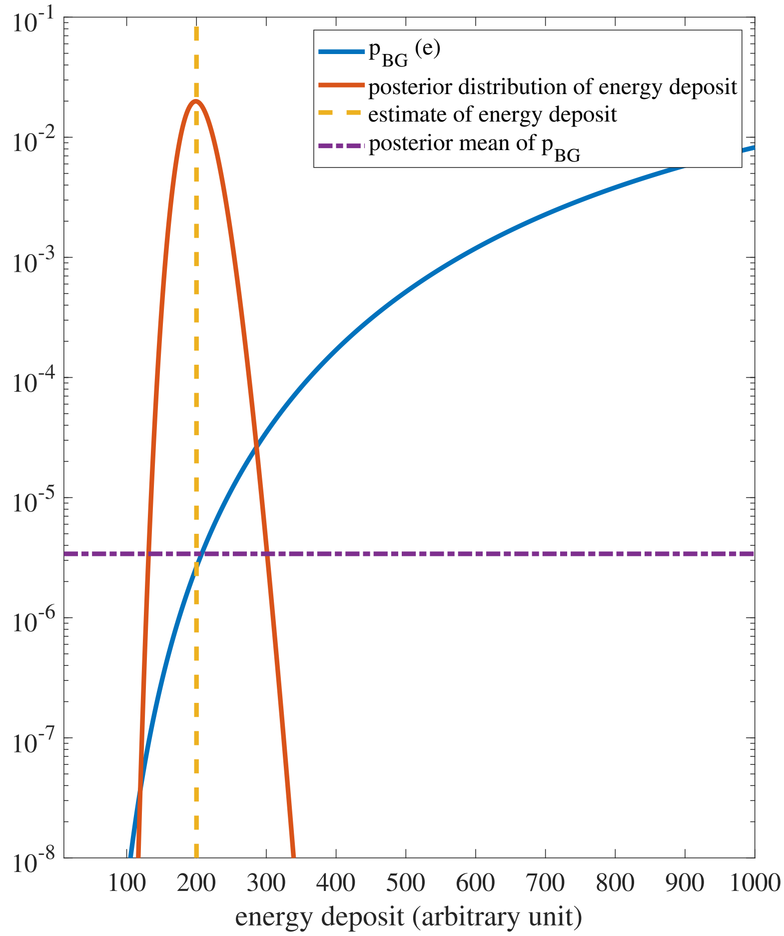

Fig. 2. Gaussian noise model where $x_t = 200$ and the discrimination threshold yields a target signal acceptance probability of 0.5. The posterior probability density function distribution of the energy deposit The posterior mean $\bar{p}_{BG}$ derived from Eq. (15), is determined with a uniform prior distribution.

Table 1. Gaussian noise model. Posterior mean of background acceptance probability and posterior mean of signal acceptance probability given that the target signal acceptance probability is 0.5. The exponential prior distribution is defined in Eq. (22).

x_t	$\bar{p}_{BG}(x_t)$ exponential prior distribution	$\bar{p}_{BG}(x_t)$ uniform prior distribution	$\bar{p}_S(x_t)$ exponential prior distribution	$\bar{p}_S(x_t)$ uniform prior distribution
100	6.11×10^{-3}	6.17×10^{-3}	0.508	0.512
200	3.31×10^{-6}	3.40×10^{-6}	0.504	0.511
300	2.47×10^{-10}	2.62×10^{-10}	0.500	0.509

2.4 Predicted Background Spectrum

In an actual experiment, one might wish to predict the background rate in each of many bins in x_t-space. For an experiment where the expected number of background events is $\mathbb{E}(N_{BG})$, the predicted number of background events that are assigned to the signal class for values of x_t in the interval $(x_k-\Delta/2, x_k+\Delta/2)$ is $\mathbb{E}(N_k)$, where

$$\mathbb{E}(N_k) \;=\; \mathbb{E}(N_{BG})\int_e\int_{x=x_k-\Delta/2}^{x_k+\Delta/2}\pi_{BG}(e)p_{BG}(x,e)f_d(x|e)dxde. \tag{23}$$

For very narrow bins in x_t-space,

$$\mathbb{E}(N_k) \;\approx\; \mathbb{E}(N_{BG})\bar{p}_{BG}(x_k)\Delta\int_e\pi_{BG}(e)f_d(x_k|e)de. \tag{24}$$

3. Poisson Noise Model

I assume that X_p and X_l are independent Poisson random variables. For the signal class, their Poisson parameters are $\lambda_p(e,S)$ and $\lambda_l(e,S)$. For the background class, their Poisson parameters are $\lambda_p(e,B)$ and $\lambda_l(e,B)$. Hence, the theoretical prompt ratios for the signal class and background class are

$$r_S(e) = \frac{\lambda_p(e,S)}{\lambda_p(e,S)+\lambda_l(e,S)}, \tag{25}$$

and

$$r_{BG}(e) = \frac{\lambda_p(e,B)}{\lambda_p(e,B)+\lambda_l(e,B)}. \tag{26}$$

Given that N_1 and N_2 are independent Poisson random variables with Poisson parameters λ_1 and λ_2 and $N=N_1+N_2$, the conditional distribution of N_1, given that the observed value of N is n, is a binomial random variable with parameters n and p where $p=\frac{\lambda_1}{\lambda_1+\lambda_2}$. This well-known result follows from the following conditional probability equality:

$$\Pr(N_1=k|N=n) = \frac{\Pr(N_1=k,N_2=n-k)}{\Pr(N=n)} = \frac{\Pr(N_1=k)\Pr(N_2=n-k)}{\Pr(N=n)}. \tag{27}$$

Thus, for the mono-energetic case, given that $X_t=x_t$, $(X_p|X_t=x_t,E=e)$ is a binomial random variable with parameters x_t and $r_S(e)$ for the signal class. For the background class, $(X_p|X_t=x_t,E=e)$ is a binomial random variable with parameters x_t and $r_{BG}(e)$.

Given that $G(k,N,p)$ is the cumulative distribution function (at k) of a binomial random variable with parameters N and p, the acceptance probabilities for the background and signal classes are

$$p_{BG}(x_t,e) = 1-G(c(x_t),x_t,r_{BG}(x_t)), \tag{28}$$

and

$$p_S(x_t,e) = 1-G(c(x_t),x_t,r_S(x_t)). \tag{29}$$

By Bayes' theorem, the posterior distribution for E given $X_t=x_t$ is

$$f_e(e|x_t) = \frac{p_d(x_t|e)\pi_{BG}(e)}{\int_e p_d(x_t|e)\pi_{BG}(e)de}, \tag{30}$$

where the conditional probability mass function of X_t given that $E = e$ is

$$p_d(X_t = x_t|e) = \frac{\exp(\,-\lambda_t(e)\,)\;\lambda_t^{x_t}(e)}{x_t!}, \tag{31}$$

where $\lambda_t(e)$ is the expected value of $(X_t|E = e)$. Based on Eqs. (28) to (31), the posterior means of the acceptance probabilities for the background class and signal class are then determined with Eq. (15) and Eq. (16).

In a simulation study, I determine posterior mean acceptance probabilities for the Poisson case (see Fig. 3; Table 2). In this study, I set $\lambda_p(e,S)$ and $\lambda_l(e,S)$ to the values of $\mu_p(e)$ and $\mu_l(e)$ assumed for the signal class in Sec. 2.3. I also set $\lambda_p(e,B)$ and $\lambda_l(e,B)$ to the values of $\mu_p(e)$ and $\mu_l(e)$ assumed for the background class in Sec. 2.3. I also set $\lambda_t(e)$ to the value of $\mu_t(e)$ assumed in Sec. 2.3. I select a threshold corresponding to a target signal acceptance of 0.5. Given x_t, this threshold is $c(x_t) = x_t r_S(e = x_t)$.

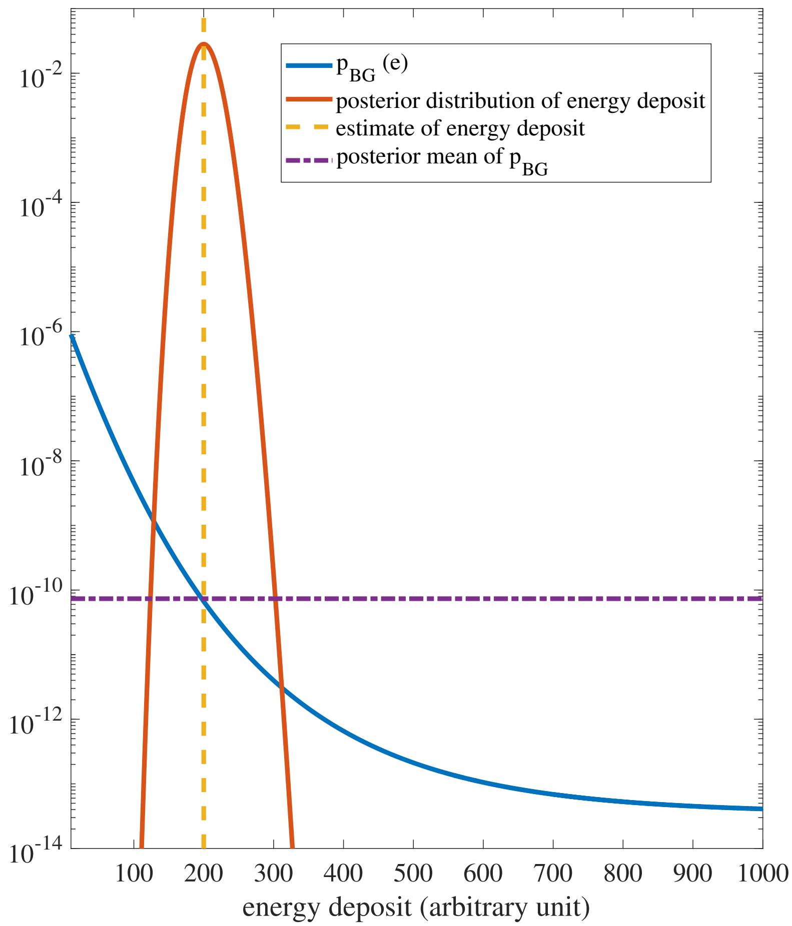

Fig. 3. Poisson noise model where $x_t = 200$ and the discrimination threshold yields a target signal acceptance probability of 0.5. The posterior mean $\bar{p}_{BG}$ derived from Eq. (15), is determined with a uniform prior distribution.

Table 2. Poisson noise model. Posterior mean of background acceptance probability and posterior mean of signal acceptance probability given that the target signal acceptance probability is 0.5. The exponential prior distribution is defined in Eq. (22).

x_t	$\bar{p}_{BG}(x_t)$ exponential prior distribution	$\bar{p}_{BG}(x_t)$ uniform prior distribution	$\bar{p}_S(x_t)$ exponential prior distribution	$\bar{p}_S(x_t)$ uniform prior distribution
100	2.34×10^{-4}	2.33×10^{-4}	0.541	0.542
200	7.45×10^{-11}	7.35×10^{-11}	0.512	0.513
300	1.27×10^{-34}	9.78×10^{-35}	0.493	0.494

3.1 Receiver-Operating-Characteristic Curve

In Fig. 4, I show how to construct a receiver-operating-characteristic (ROC) curve for any particular value of x_t for the Poisson noise model. In this study, $x_t = 100$ and the theoretical model for the Poisson parameters for the prompt and late time intervals for the signal and background are the same as discussed earlier. In Eq. (28) and Eq. (29), the discrimination threshold, $c(x_t)$, is varied over a broad range of integer values (20 to 83). For each candidate discrimination threshold, I determine the posterior mean value of $p_{BG}(x_t, e)$ and the posterior mean value of $p_S(x_t, e)$ (see Figs. 4a and 4b). Each candidate discrimination threshold yields a distinct value of $(\bar{p}_{BG}(x_t), \bar{p}_S(x_t))$. The ROC curve is the union of all distinct values of $(\bar{p}_{BG}(x_t), \bar{p}_S(x_t))$ (see Figs. 4c and 4d). One can construct an ROC curve for the Gaussian noise model with a similar approach.

4. Discussion

For both the Poisson and Gaussian models, for any particular energy deposit, I assume that X_p and X_l are independent random variables (see Sec. 2.1 and Sec. 3). As discussed earlier (see Sec. 1), in many experiments, only a fraction of the full energy deposit produces measurements of interest. As remarked earlier, I assume in this work that this fraction does not vary from event-to-event for each class. If this fraction randomly varies from event-to-event, I expect X_p and X_l to be positively correlated for any particular energy deposit. The models in this work do not account for this correlation structure.

In the simulations reported here, the posterior mean of the background acceptance probability increases as the energy deposit increases for the Gaussian model (see Fig. 2). In contrast, for the Poisson model, the posterior mean of the background acceptance probability decreases as the energy deposit increases (see Fig. 3). I attribute this result to the fact that the fractional standard deviation (standard deviation divided by expected value) of the conditional value of X_p is larger for the Gaussian case relative to the Poisson case.

The choice of prior distribution affected results slightly (see Tables 1 and 2). As a caveat, there may be other prior distributions of interest.

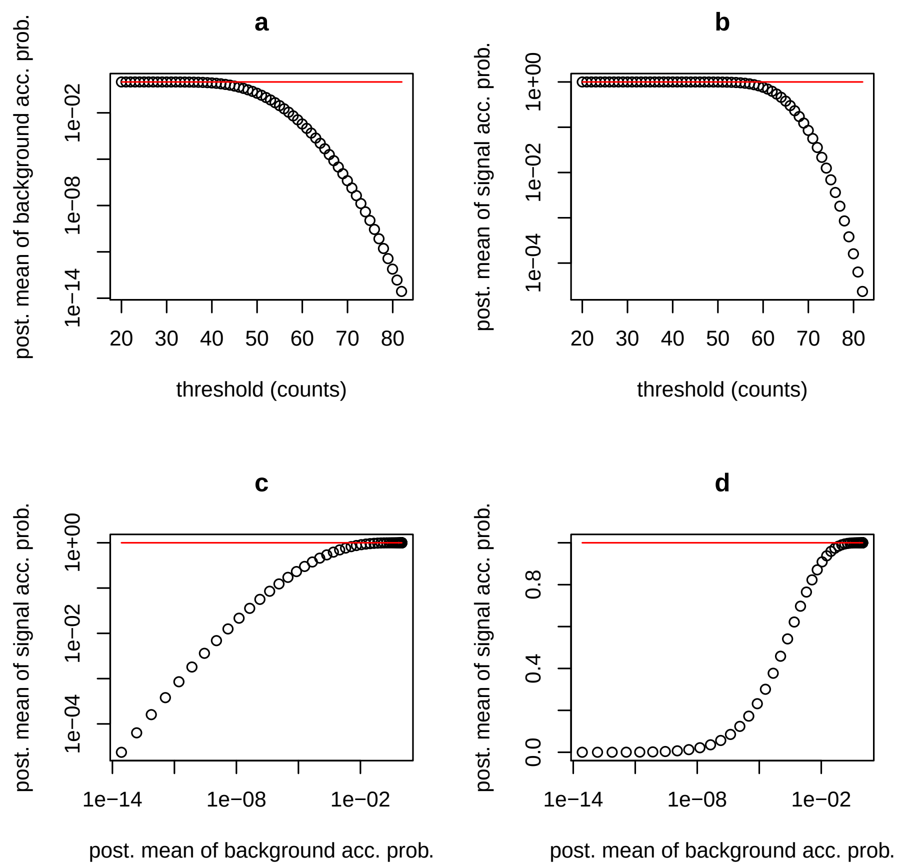

Fig. 4. Poisson noise model where $x_t = 100$. (a) Posterior (post.) mean of background acceptance probability (acc. prob.) ($\bar{p}_{BG}$) versus discrimination threshold. (b) Posterior mean of signal acceptance probability ($\bar{p}_S$) versus discrimination threshold. (c) ROC curve ($\bar{p}_S$ versus $\bar{p}_{bg}$) on log-log scale. (d) ROC curve on log-linear scale. Posterior means are determined with a uniform prior distribution. The horizontal line corresponds to 1.

5. Summary

In this theoretical study, I derived analytical expressions that quantify the performance of a ratio-based pulse shape discrimination method for Gaussian and Poisson noise models. With a Bayesian method, for a particular target acceptance probability for the signal class events, I determined the posterior mean background acceptance probability as a function of the observed value of X_t in a way that accounted for imperfect knowledge of the energy deposit. In a simulation study, I determined results for two choices of the prior distribution in the Bayesian method (see Tables 1 and 2).

My analytic methods may enable one to determine receiver-operating-characteristic curves by numerical integration rather than by Monte Carlo simulation. My methods may provide experimentalists with useful theoretical predictions of ratio-based PSD performance in planning studies provided that integrated pulses are well approximated as realizations of either Gaussian random variables or Poisson random variables, and accurate models for the energy-dependent distributions of X_p and X_t are available for background events and signal events.

Acknowledgments

I thank H.-K. Liu, M.S. Dewey and P. Mumm of NIST for helpful comments. Contributions by staff of NIST, an agency of the US government, are not subject to copyright in the United States.

6. References

[1] Borexino Collaboration Alimonti G, Arpesella C, Back H, Balata M, Beau T, Bellini G, Benziger J, Bonetti S, Brigatti A, Caccianiga B, Cadonati L, Calaprice F, Cecchet G, Chen M, DeBari A, DeHaas E, de Kerret H, Donghi O, Deutsch M, Elisei F, Etenko A, von Feilitzsch F, Fernholz R, Ford R, Freudiger B, Garagiola A, Galbiati C, Gatti F, Gazzana S, Giammarchi M, Giugni D, Golubchikov A, Goretti A, Grieb C, Hagner C, Hagner T, Hampel W, Harding E, Hartmann F, von Hentig R, Hess H, Heusser G, Ianni A, Inzani P, Kidner S, Kiko J, Kirsten T, Korga G, Korschinek G, Kryn D, Lagomarsino V, LaMarche P, Laubenstein M, Loeser F, Lombardi P, Magni S, Malvezzi S, Maniera J, Manno I, Manuzio G, Masetti F, Mazzucato U, Meroni E, Musico P, Neder H, Neff M, Nisi S, Oberauer L, Obolensky M, Pallavicini M, Papp L, Perasso L, Pocar A, Raghavan R, Ranucci G, Rau W, Razeto A, Resconi E, Riedel T, Sabelnikov A, Saggese P, Salvo C, Scardaoni R, Schoenert S, Schuhbeck K, Seidel H, Shutt T, Simgen H, Sonnenschein A, Smirnov O, Sotnikov A, Skorokhvatov M, Sukhotin S, Tartaglia R, Testera G, Vogelaar R, Vitale S, Wojcik M, Zaimidoroga O, Zakharov Y (2002) Science and technology of Borexino: A real-time detector for low energy solar neutrinos. *Astroparticle Physics* 16(3):205–234. https://doi.org/10.1016/S0927-6505(01)00110-4

[2] Lippincott W, Coakley KJ, Gastler D, Hime A, Kearns E, McKinsey D, Nikkel J, Stonehill L (2008) Scintillation time dependence and pulse shape discrimination in liquid argon. *Physical Review C* 78(3):035801. https://doi.org/10.1103/PhysRevC.78.035801

[3] Ueshima K, Abe K, Hiraide K, Hirano S, Kishimoto Y, Kobayashi K, Koshio Y, Liu J, Martens K, Moriyama S, Nakahata M, Nishiie H, Ogawa H, Sekiya H, Shinozaki A, Suzuki Y, Takeda A, Yamashita M, Fujii K, Murayama I, Nakamura S, Otsuka K, Takeuchi Y, Fukuda Y, Nishijima K, Motoki D, Itow Y, Masuda K, Nishitani Y, Uchida H, Tasaka S, Ohsumi H, Kim YD, Kim YH, Lee KB, Lee MK, Lee JS, The XMASS Collaboration (2011) Scintillation-only based pulse shape discrimination for nuclear and electron recoils in liquid xenon. *Nuclear Instruments and Methods in Physics Research Section A: Accelerators, Spectrometers, Detectors and Associated Equipment* 659(1):161–168. https://doi.org/10.1016/j.nima.2011.09.011

[4] O'Keeffe H, O'Sullivan E, Chen M (2011) Scintillation decay time and pulse shape discrimination in oxygenated and deoxygenated solutions of linear alkylbenzene for the SNO+ experiment. *Nuclear Instruments and Methods in Physics Research Section A: Accelerators, Spectrometers, Detectors and Associated Equipment* 640(1):119–122. https://doi.org/10.1016/j.nima.2011.03.027

[5] Amaudruz PA, Batygov M, Beltran B, Bonatt J, Boudjemline K, Boulay MG, Broerman B, Bueno J, Butcher A, Cai B, Caldwell T, Chen M, Chouinard R, Cleveland BT, Cranshaw D, Dering K, Duncan F, Fatemighomi N, Ford R, Gagnon R, Giampa P, Giuliani F, Gold M, Golovko VV, Gorel P, Grace E, Graham K, Grant DR, Hakobyan R, Hallin AL, Hamstra M, Harvey P, Hearns C, Hofgartner J, Jillings CJ, Kuźniak M; Lawson I, La Zia F, Li O, Lidgard JJ, Liimatainen P, Lippincott WH, Mathew R, McDonald AB, McElroy T, McFarlane K, McKinsey DN, Mehdiyev R, Monroe J, Muir A, Nantais C, Nicolics K, Nikkel J, Noble AJ, O'Dwyer E, Olsen K, Ouellet C, Pasuthip P, Peeters SJM, Pollmann T, Rau W, Retière F, Ronquest M, Seeburn N, Skensved P, Smith B, Sonley T, Tang J, Vázquez-Jáuregui E, Veloce L, Walding J, Ward M (2016) Measurement of the scintillation time spectra and pulse-shape discrimination of low-energy β and nuclear recoils in liquid argon with DEAP-1. *Astroparticle Physics* 85:1–23. https://doi.org/10.1016/j.astropartphys.2016.09.002

[6] Calvo J, Cantini C, Crivelli P, Daniel M, Di Luise S, Gendotti A, Horikawa S, Molina-Bueno L, Montes B, Mu W, Murphy S, Natterer G, Nguyen K, Periale L, Quan Y, Radics B, Regenfus C, Romero L, Rubbia A, Santorelli R, Sergiampietri F, Viant T, Wu (2018) Backgrounds and pulse shape discrimination in the ArDM liquid argon TPC. *Journal of Cosmology and Astroparticle Physics* 2018(12):011. https://doi.org/10.1088/1475-7516/2018/12/011

[7] Klein H, Neumann S (2002) Neutron and photon spectrometry with liquid scintillation detectors in mixed fields. *Nuclear Instruments and Methods in Physics Research Section A: Accelerators, Spectrometers, Detectors and Associated Equipment* 476(1-2):132–142. https://doi.org/10.1016/S0168-9002(01)01410-3

[8] Flaska M, Pozzi SA (2007) Identification of shielded neutron sources with the liquid scintillator BC-501A using a digital pulse shape discrimination method. *Nuclear Instruments and Methods in Physics Research Section A: Accelerators, Spectrometers, Detectors and Associated Equipment* 577(3):654–663. https://doi.org/10.1016/j.nima.2007.04.141

[9] Fisher B, Abdurashitov J, Coakley K, Gavrin V, Gilliam D, Nico J, Shikhin A, Thompson A, Vecchia D, Yants V (2011) Fast neutron detection with ^{6}Li-loaded liquid scintillator. *Nuclear Instruments and Methods in Physics Research Section A: Accelerators, Spectrometers, Detectors and Associated Equipment* 646(1):126–134. https://doi.org/10.1016/j.nima.2011.04.019

[10] Zaitseva N, Rupert BL, PaweŁczak I, Glenn A, Martinez HP, Carman L, Faust M, Cherepy N, Payne S (2012) Plastic scintillators with efficient neutron/gamma pulse shape discrimination. *Nuclear Instruments and Methods in Physics Research Section A: Accelerators, Spectrometers, Detectors and Associated Equipment* 668:88–93. https://doi.org/10.1016/j.nima.2011.11.071

[11] Elliott S, Gehman V, Kazkaz K, Mei DM, Young A (2006) Pulse shape analysis in segmented detectors as a technique for background reduction in Ge double-beta decay experiments. *Nuclear Instruments and Methods in Physics Research Section A: Accelerators, Spectrometers, Detectors and Associated Equipment* 558(2):504–510. https://doi.org/10.1016/j.nima.2005.12.024

[12] Almazán H, del Amo Sanchez P, Bernard L, Blanchet A, Bonhomme A, Buck C, Favier J, Haser J, Hélaine V, Kandzia F, Kox S, Lamblin J, Letourneau A, Lhuillier D, Lindner M, Manzanillas L, Materna T, Minotti A, Montanet F, Pessard H, Real J-S, Roca C, Salagnac T, Schoppmann S, Sergeyeva V, Soldner T, Stutz A, Zsoldos S (2018) Sterile neutrino constraints from the STEREO experiment with 66 days of reactor-on data. *Physical Review Letters* 121(16):161801. https://doi.org/10.1103/PhysRevLett.121.161801

[13] Andriamirado M, Balantekin A, Band H, Bass C, Bergeron D, Berish D, Bowden N, Brodsky J, Bryan C, Classen T, Conant AJ, Deichert G, Diwan MV, Dolinski MJ, Erickson A, Foust BT, Gaison JK, Galindo-Uribarri, Gilbert CE, Goddard BW, Hackett BT, Hans A, Hansell AB, Heeger KM, Jaffe DE, Ji X, Jones DC, Kyzylova O, Lane CE, Langford TJ, LaRosa J, Littlejohn BR, Lu X, Maricic J, Mendenhall MP, Meyer AM, Milincic R, Mitchell I, Mueller PE, Mumm HP, Napolitano J, Nave C, Neilson R, Nikkel JA, Norcini D, Nour S, Palomino JL, Pushin DA, Qian X, Romero-Romero E, Rosero R, Surukuchi PT, Tyra MA, Varner RL, Venegas-Vargas D, Weatherly PB, White C, Wilhelmi J, Woolverton A, Yeh M, Zhang A, Zhang C, Zhang X (PROSPECT Collaboration) (2021) Improved short-baseline neutrino oscillation search and energy spectrum measurement with the PROSPECT experiment at HFIR. *Physical Review D* 103(3):032001. https://doi.org/10.1103/PhysRevD.103.032001

[14] Balmer MJ, Gamage KA, Taylor GC (2015) Comparative analysis of pulse shape discrimination methods in a ^{6}Li loaded plastic scintillator. *Nuclear Instruments and Methods in Physics Research Section A: Accelerators, Spectrometers, Detectors and Associated Equipment* 788:146–153. https://doi.org/10.1016/j.nima.2015.03.089

[15] Monterial M, Marleau P, Clarke S, Pozzi S (2015) Application of Bayes' theorem for pulse shape discrimination. *Nuclear Instruments and Methods in Physics Research Section A: Accelerators, Spectrometers, Detectors and Associated Equipment* 795:318–324. https://doi.org/10.1016/j.nima.2015.06.014

[16] Hawkes N, Gamage K, Taylor G (2010) Digital approaches to field neutron spectrometry. *Radiation Measurements* 45(10):1305–1308. https://doi.org/10.1016/j.radmeas.2010.06.043

[17] The n_TOF Collaboration, Marrone S, Cano-Ott D, Colonna N, Domingo C, Gramegna F, Gonzalez E, Gunsing F, Heil M, Käppeler F, Mastinu P, Milazzo PM, Papaevangelou T, Pavlopoulos P, Plag R, Reifarth R, Tagliente G, Tain JL, Wisshak K (2002) Pulse shape analysis of liquid scintillators for neutron studies. *Nuclear Instruments and Methods in Physics Research Section A: Accelerators, Spectrometers, Detectors and Associated Equipment* 490(1-2):299–307. https://doi.org/10.1016/S0168-9002(02)01063-X

[18] Guerrero C, Cano-Ott D, Fernandez-Ordonez M, González-Romero E, Martínez T, Villamarín D (2008) Analysis of the BC501A neutron detector signals using the true pulse shape. *Nuclear Instruments and Methods in Physics Research Section A: Accelerators, Spectrometers, Detectors and Associated Equipment* 597(2-3):212–218. https://doi.org/10.1016/j.nima.2008.09.017

[19] Liu G, Aspinall M, Ma X, Joyce M (2009) An investigation of the digital discrimination of neutrons and γ rays with organic scintillation detectors using an artificial neural network. *Nuclear Instruments and Methods in Physics Research Section A: Accelerators, Spectrometers, Detectors and Associated Equipment* 607(3):620–628. https://doi.org/10.1016/j.nima.2009.06.027

[20] Sanderson T, Scott C, Flaska M, Polack J, Pozzi S (2012) Machine learning for digital pulse shape discrimination. *2012 IEEE Nuclear Science Symposium and Medical Imaging Conference Record (NSS/MIC)* (IEEE), pp 199–202. https://doi.org/10.1109/NSSMIC.2012.6551092

[21] Mace EK, Ward JD, Aalseth C (2018) Use of neural networks to analyze pulse shape data in low-background detectors. *Journal of Radioanalytical and Nuclear Chemistry* 318(1):117–124. https://doi.org/10.1007/s10967-018-5983-1

[22] Holl P, Hauertmann L, Majorovits B, Schulz O, Schuster M, Zsigmond A (2019) Deep learning based pulse shape discrimination for germanium detectors. *The European Physical Journal C* 79(6):1–9. https://doi.org/10.1140/epjc/s10052-019-6869-2

[23] Zhang Z, Hu C, Zhang Y, Liao B, Zhu J, Fan X, Li Y, Zhang L (2019) The combined application of principal component analysis and decision tree in nuclear pulse shape discrimination. *Nuclear Instruments and Methods in Physics Research Section A: Accelerators, Spectrometers, Detectors and Associated Equipment* 943:162425. https://doi.org/10.1016/j.nima.2019.162425

[24] Griffiths J, Kleinegesse S, Saunders D, Taylor R, Vacheret A (2020) Pulse shape discrimination and exploration of scintillation signals using convolutional neural networks. *Machine Learning: Science and Technology* 1(4):045022. https://doi.org/10.1088/2632-2153/abb781

[25] Gelfusa M, Rossi R, Lungaroni M, Belli F, Spolladore L, Wyss I, Gaudio P, Murari A, JET Contributors (2020) Advanced pulse shape discrimination via machine learning for applications in thermonuclear fusion. *Nuclear Instruments and Methods in Physics Research Section A: Accelerators, Spectrometers, Detectors and Associated Equipment* 974:164198. https://doi.org/10.1016/j.nima.2020.164198

[26] D'Mellow B, Aspinall M, Mackin R, Joyce MJ, Peyton A (2007) Digital discrimination of neutrons and γ-rays in liquid scintillators using pulse gradient analysis. *Nuclear Instruments and Methods in Physics Research Section A: Accelerators, Spectrometers, Detectors and Associated Equipment* 578(1):191–197. https://doi.org/10.1016/j.nima.2007.04.174

[27] Roush ML, Wilson M, Hornyak WF (1964) Pulse shape discrimination. *Nuclear Instruments and Methods* 31(1):112–124. https://doi.org/10.1016/0029-554X(64)90333-7

[28] Wolski D, Moszyński M, Ludziejewski T, Johnson A, Klamra W, Skeppstedt Ö (1995) Comparison of n-γ discrimination by zero-crossing and digital charge comparison methods. *Nuclear Instruments and Methods in Physics Research Section A: Accelerators, Spectrometers, Detectors and Associated Equipment* 360(3):584–592. https://doi.org/10.1016/0168-9002(95)00037-2

[29] Liu G, Joyce MJ, Ma X, Aspinall MD (2010) A digital method for the discrimination of neutrons and γ rays with organic scintillation detectors using frequency gradient analysis. *IEEE Transactions on Nuclear Science* 57(3):1682–1691. https://doi.org/10.1109/TNS.2010.2044246

[30] Safari M, Davani FA, Afarideh H, Jamili S, Bayat E (2016) Discrete Fourier transform method for discrimination of digital scintillation pulses in mixed neutron-gamma fields. *IEEE Transactions on Nuclear Science* 63(1):325–332. https://doi.org/10.1109/TNS.2016.2514400

[31] Hinkley DV (1969) On the ratio of two correlated normal random variables. *Biometrika* 56(3):635–639. https://doi.org/10.1093/biomet/56.3.635

[32] Hinkley DV (1970) Correction: On the ratio of two correlated normal random variables. *Biometrika* 57(3):683. https://doi.org/10.1093/biomet/57.3.683

[33] Marsaglia G (1965) Ratios of normal variables and ratios of sums of uniform variables. *Journal of the American Statistical Association* 60(309):193–204. https://doi.org/10.1080/01621459.1965.10480783

[34] Lidgard JJ (2008) *Pulse Shape Discrimination Studies in Liquid Argon for the DEAP-1 Detector* (Queen's University, Kingston, Ontario, Canada).

[35] Fawcett T (2006) An introduction to ROC analysis. *Pattern Recognition Letters* 27(8):861–874. https://doi.org/10.1016/j.patrec.2005.10.010

[36] Eaton ML (1983) *Multivariate Statistics: a Vector Space Approach* (John Wiley & Sons, Inc., New York), 512p. https://www.jstor.org/stable/i20461447

[37] Gelman A, Carlin JB, Stern HS, Dunson DB, Vehtari A, Rubin DB (2013) *Bayesian Data Analysis* (CRC Press, Boca Raton, FL). https://doi.org/10.1201/b16018

About the author: *Kevin J Coakley is a mathematical statistician in the Statistical Engineering Division of the Information Technology Laboratory at the National Institute of Standards and Technology in Boulder, CO. He earned a PhD in statistics from Stanford University. The National Institute of Standards and Technology is an agency of the U.S. Department of Commerce.*